Short Communication Wiley Online Library ELECTROANALYSIS

DOI: 10.1002/elan.201800209

Electrocatalytic Activity of Nanohybrids Based on Carbon Nanomaterials and MFe_2O_4 (M = Co, Mn) towards the Reduction of Hydrogen Peroxide

Fabiana A. Gutierrez,[a] Eva Mazario,[b] Nieves Menéndez,[b] Pilar Herrasti,[b] María D. Rubianes,[a] José H. Zagal,[c] C. Yañez,[d] Gustavo A. Rivas,*[a] Soledad Bollo,*[d, e] and F. Javier Recio*[f, g]

Abstract: We report the advantages of hybrid nanomaterials prepared with electrogenerated ferrites (MFe_2O_4; M: Co, Mn) and multi-walled carbon nanotubes (MWCNTs) or thermally reduced graphene oxide (TRGO) on the electro-reduction of hydrogen peroxide. Glassy carbon electrodes (GCE) modified with these hybrid nanomaterials dispersed in Nafion/isopropanol demonstrated a clear synergism on the catalytic reduction of reduction of hydrogen peroxide at pH 13.00. The intimate interaction between MFe_2O_4 and carbon nanomaterials allowed a better electronic transfer and a facilitated regeneration of M^{2+} at the carbon nanomaterials, reducing the charge transfer resistances for hydrogen peroxide reduction and increasing the sensitivities of the amperometric response.

Keywords: Cobalt · Manganese · Ferrites · Carbon nanotubes · Graphene · Hybrid nanomaterials · Hydrogen peroxide · Electrocatalysis

Hydrogen peroxide is a key metabolite intimately related to several metabolic pathways and is widely used in food, pharmaceutical, chemical and biochemical industries [1,2]. The study of the electroreduction of hydrogen peroxide has received considerable attention mainly due to the importance of the development of oxidases-based biosensors, non-enzymatic sensors and fuel cells. Taking into account that the reduction of hydrogen peroxide at conventional electrodes requires elevated overvoltages, one of the key aspects is the development of materials that allow the decrease of these overvoltages. In this regard, several alternatives have been proposed [3,6]. Among them, the use of metals and metal oxides have received considerable attention. In fact, metals like rhodium, copper, platinum, gold or their combination [7–16]; metal oxides such as copper oxide, manganese oxide [17–21]; perovskites [22–23] and electrogenerated ferrites [24–26] have been successfully used for this task.

Spinel ferrites present unique electronic, optical, magnetic and catalytic properties that make them very interesting nanomaterials [27]. The electrogenerated ones have interesting properties associated with the possibility to tune their size and composition [28,29]. Carbon nanotubes (CNTs) have demonstrated to present additional advantages mainly connected with their high surface-to-volume ratio, their unique electronic properties and the presence of edge-plane like defects that make them a very interesting material for electroanalytical applications [30,31]. Since 2004, graphene has received enormous attention due to its high thermal conductivity, high electron mobility at room temperature, capacity to maintain high current densities, and easy functionalization, among others [32]. Both carbon nanomaterials have been widely used in the field of electroanalysis as the explosive increase in the number of papers have demonstrated. Hybrid nanomaterials prepared by association of carbon nanostructures and different nanoparticles have demonstrated better performances than similar configurations using the individual components as a consequence of the combined properties or synergistic effect of the individual materials [33–35]. Madhura et al. [36] have reported the synergism between $MnFe_2O_4$ and reduced

[a] F. A. Gutierrez, M. D. Rubianes, G. A. Rivas
INFIQC (UNC-CONICET), Departamento de Fisicoquímica, Facultad de Ciencias Químicas, Universidad Nacional de Córdoba, Argentina
E-mail: grivas@fcq.unc.edu.ar
[b] E. Mazario, N. Menéndez, P. Herrasti
Departamento de Química Física Aplicada, Facultad de Ciencias Químicas, Universidad Autónoma Madrid, España
[c] J. H. Zagal
Departamento de Química de los Materiales, Facultad de Química y Biología, Universidad de Santiago de Chile, Av. Libertador B. O'Higgins 3363, Casilla 40, Correo 33, Santiago, Chile
[d] C. Yañez, S. Bollo
CiPRex, Facultad de Ciencias Químicas y Farmacéuticas
[e] S. Bollo
Advanced Center for Chronic Diseases (ACCDiS), Universidad de Chile, Chile
E-mail: sbollo@ciq.uchile.cl
[f] F. J. Recio
Departamento de Química Inorgánica, Facultad de Química
[g] F. J. Recio
Centro de Nanotecnología y Materiales Avanzados. CIEN-UC, Pontificia Universidad Católica de Chile, Chile
E-mail: javier.recio@uc.cl

graphene oxide (rGO) nanohybrids on the catalytic reduction of hydrogen peroxide. Ensafi et al. [37] have proposed the use of glassy carbon electrodes (GCE) modified with exfoliated GO decorated with $CoFe_2O_4$ for the quantification of hydrogen peroxide and NADH, reporting a synergistic effect as a result of the combination of the nanomaterials. Teymourian et al. [38] have reported the electrocatalytic activity of nanocomposites constituted by Fe_3O_4 magnetic nanoparticles and rGO nanosheets towards the reduction of hydrogen peroxide and O_2 and the oxidation of NADH.

In this work we report the catalytic activity of hybrid nanomaterials obtained by combination of electrogenerated nanosized ferrites (MFe_2O_4, where M: Mn and Co) and multi-walled carbon nanotubes (MWCNTs) or thermally reduced graphene oxide (TRGO) towards the reduction of hydrogen peroxide at pH 13.00. In the following sections, we perform a critical comparison of the catalytic activity towards the reduction of hydrogen peroxide for glassy carbon electrodes (GCE) modified with the nanohybrids (MWCNTs-MFe_2O_4 and TRGO-MFe_2O_4) and the individual nanomaterials (MWCNTs, TRGO and MFe_2O_4) dispersed in Nafion/isopropanol/water (Naf-IP).

Figure 1 shows TEM micrographs of the electrogenerated $CoFe_2O_4$ (A) and $MnFe_2O_4$ (B) nanoparticles (NP). Both NPs present almost spherical shapes and, according to the histograms displayed in the insets (N = 100 NP), the sizes are (18 ± 3) nm and (19 ± 3) nm for $CoFe_2O_4$ and $MnFe_2O_4$, respectively. These values are in agreement with those obtained from X-ray diffraction patterns (not shown).

Figure 2 compares the polarization curves obtained for 1.0×10^{-2} M hydrogen peroxide at GCE and GCE modified with different materials, either carbon nanostructures (TRGO or MWCNTs), ferrites ($CoFe_2O_4$ and $MnFe_2O_4$), or hybrids carbon nanomaterial/ferrite (MWCNTs-$CoFe_2O_4$, MWCNTs-$MnFe_2O_4$, TRGO-$CoFe_2O_4$ and TRGO-$MnFe_2O_4$). Figure 2A displays the polarization curves for hydrogen peroxide at GCE (black), GCE/MWCNTs (red) and GCE/TRGO (green). The presence of TRGO and MWCNTs at the glassy carbon surface produces a decrease on the onset potentials for the reduction of hydrogen peroxide (87 and 25 mV, respectively) and an increase of the maxima hydrogen peroxide reduction currents (13 and 6 μA for GCE/MWCNTs and GCE/TRGO) compared to GCE (maximum current 4 μA). The modification of GCE with $CoFe_2O_4$ (Figure 2B, blue) or $MnFe_2O_4$ (Figure 2C, blue), produced a decrease in the onset potentials for hydrogen peroxide reduction similar to that observed in the presence of the carbon nanomaterials (compared to GCE). The associated currents show an enhancement even more pronounced that in the case of GCE/carbon nanomaterials (32 and 24 μA for GCE/$CoFe_2O_4$ and GCE/$MnFe_2O_4$, respectively), clearly indicating the catalytic activity of the ferrites towards the reduction of hydrogen peroxide. The analysis of the polarization curves for GCE modified with

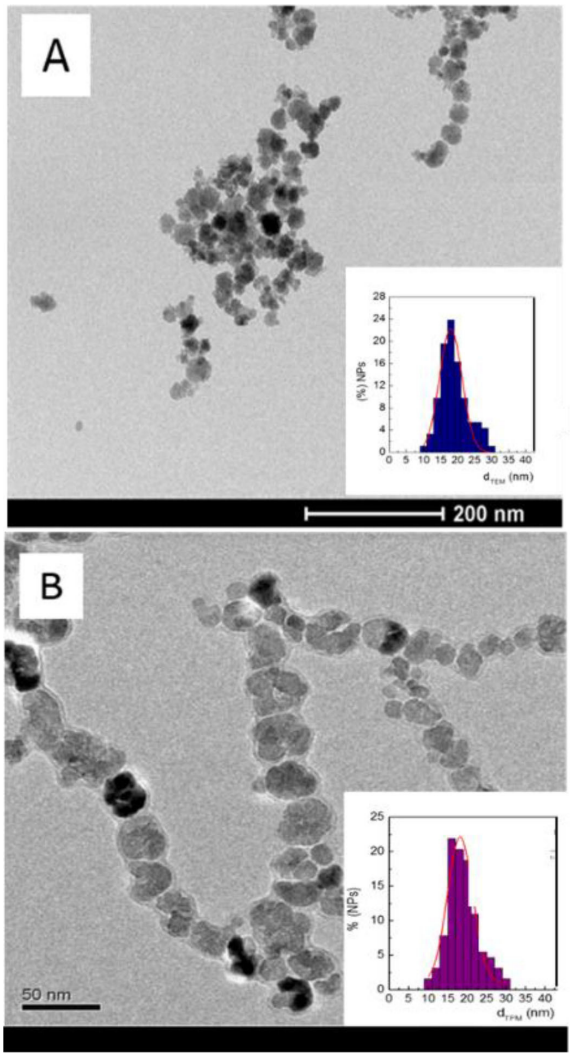

Fig. 1. TEM images of $CoFe_2O_4$ (A) and $MnFe_2O_4$ (B). The inset shows size histograms (N = 100 NP).

the nanohybrids (GCE/MWCNTs-$CoFe_2O_4$ (Figure 2B, red), GCE/TRGO-$CoFe_2O_4$ (Figure 2B, green), GCE/MWCNTs-$MnFe_2O_4$ (Figure 2C, red), and GCE/TRGO-$MnFe_2O_4$ (Figure 2C, green)) indicates that the onset potentials for hydrogen peroxide reduction do not present significant changes compared to GCE/ferrites. However, the reduction currents largely increase compared to GCE/ferrites and GCE/carbon nanomaterials (106, 58, 92 and 50 μA for GCE/MWCNTs-$CoFe_2O_4$, GCE/TRGO-$CoFe_2O_4$, GCE/MWCNTs-$MnFe_2O_4$, and GCE/TRGO-$MnFe_2O_4$, respectively). These profiles are a clear evidence of the catalytic behavior of MFe_2O_4 towards the reduction of hydrogen peroxide mediated by the nanoparticle metallic center (Co or Mn) and the synergism between the nanomaterials.

Tafel plots for the different systems are presented as insets of Figures 2A, B and C. The slopes for GCE/$CoFe_2O_4$, GCE/$MnFe_2O_4$, GCE/MWCNTs-$CoFe_2O_4$, GCE/MWCNTs-$MnFe_2O_4$, GCE/TRGO-$CoFe_2O_4$ and

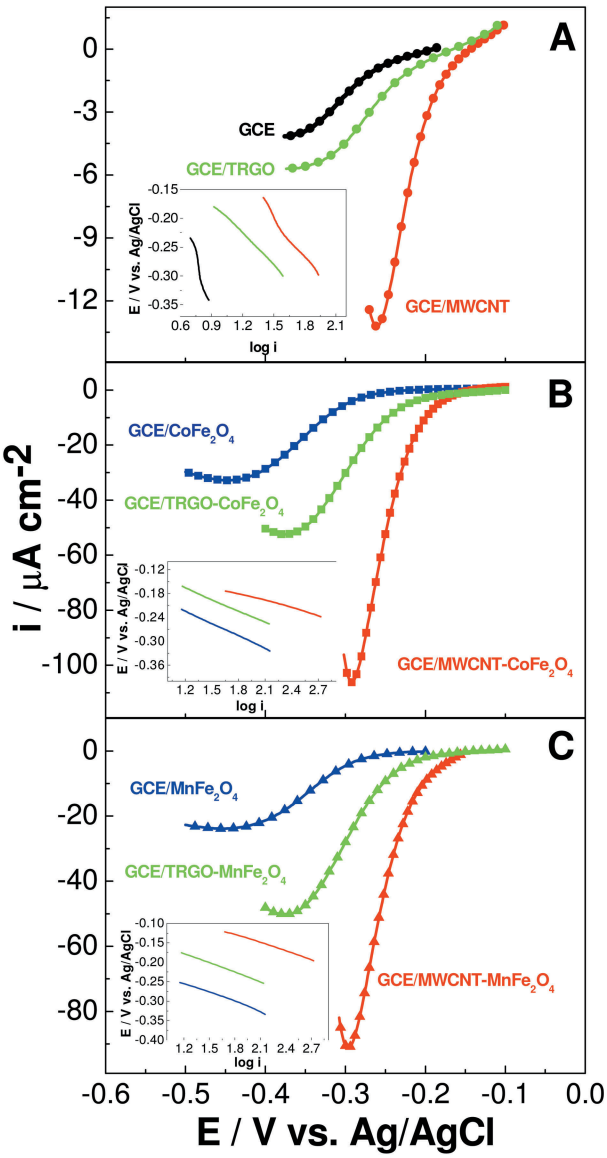

Fig. 2. Polarization curves for 1.0×10^{-2} M hydrogen peroxide prepared in 0.100 M NaOH, pH 13.00 obtained at: (A) GCE (black), GCE/TRGO (green) and GCE/MWCNT (red); (B) GCE/$CoFe_2O_4$ (blue), GCE/TRGO-$CoFe_2O_4$ (green) and GCE/MWCNT-$CoFe_2O_4$ (red); C) GCE/$MnFe_2O_4$ (blue), GCE/TRGO-$MnFe_2O_4$ (green) and GCE/MWCNT-$MnFe_2O_4$ (red). Inset show the corresponding semilogaritmic Tafel plots.

GCE/TRGO-$MnFe_2O_4$ are $-(0.063\pm0.005)$, $-(0.063\pm0.004)$, $-(0.059\pm0.002)$, $-(0.058\pm0.009)$, $-(0.059\pm0.003)$, and $-(0.058\pm0.002)$ $Vdec^{-1}$, respectively, that is, the Tafel slopes for all the electrodes modified with ferrites, either alone of associated with MWCNTs or TRGO, are around 0.059 $Vdec^{-1}$. On the contrary, in the absence of MFe_2O_4, the Tafel slopes are higher: $-(0.11\pm0.01)$ $Vdec^{-1}$; $(-(0.130\pm0.009)$ $Vdec^{-1}$ and $(-(0.11\pm0.06)$ $Vdec^{-1}$ for GCE; GCE/TRGO and GCE/MWCNTs, respectively. These values of Tafel slopes indicate that when the ferrites are present at the electrode surface, the catalytic reduction of hydrogen peroxide is mediated by M^{2+}, while in the absence of ferrites the determining rate step is the charge transfer at the carbon materials.

To obtain complementary information about the electrochemical behavior of hydrogen peroxide at the different electrodes, we performed EIS experiments for GCE, GCE modified with the individual nanomaterials (MWCNTs, TRGO, $CoFe_2O_4$ and $MnFe_2O_4$) and GCE modified with the hybrid nanomaterials (GCE/MWCNTs/$MnFe_2O_4$, GCE/MWCNTs/$CoFe_2O_4$, GCE/TRGO/$CoFe_2O_4$ and GCE/TRGO/$MnFe_2O_4$). The experimental data for GCE, GCE/TRGO and GCE/MFe_2O_4 were fitted with a ($R_s(R_{ct}C_{dl})$) circuit, where R_s is the electrolytic resistance, R_{ct} the charge transfer resistance and C_{dl} the double layer capacitance. It the case of GCE modified with the hybrid nanomaterials the systems were fitted using an equivalent circuit with two additional elements, a capacitance (C_2) and a resistance (R_2) associated with the electrocatalytic activity of the carbon nanomaterials ($R_s(R_1C_1)(R_2C_2)$). Every (R_nC_n) represent one time-constant, associated with each nanomaterial present in the hybrid. In the particular case of GCE/MWCNT, the data were also fitted with the second circuit, since two time-constants are present, probably due to the existence of some residual impurities in the MWCNT. Figure 3A shows Nyquist diagrams obtained for 1.0×10^{-2} M hydrogen peroxide at GCE/Naf-IP (a), GCE/$MnFe_2O_4$ (b) and GCE/$CoFe_2O_4$ (c). The presence of MFe_2O_4 produces a huge decrease of R_{ct} due to their catalytic activity towards the reduction of hydrogen peroxide. In fact, R_{ct} decreases from $(1.08\pm0.04)\times10^5$ Ω at GCE/Naf-IP to $(1.1\pm0.1)\times10^4$ and $(1.2\pm0.3)\times10^4$ Ω at GCE/$CoFe_2O_4$ and GCE/$MnFe_2O_4$, respectively. The analysis of Figures 3B and 3C indicate that the modification of GCE with the hybrid nanomaterials produces a drastic decrease in R_{ct} compared either to GCE/carbon nanomaterial or GCE/MFe_2O_4, reaching values of $(1.2\pm0.5)\times10^3$ and $(2.7\pm0.5)\times10^3$ Ω for GCE/MWCNT-$CoFe_2O_4$ and GCE/MWCNT-$MnFe_2O_4$, respectively (Figure 3B); and $(1.7\pm0.5)\times10^3$ and $(3.5\pm0.5)\times10^3$ Ω for GCE/TRGO-$CoFe_2O_4$ and GCE/TRGO-$MnFe_2O_4$, respectively (Figure 3C). Therefore, the modification of GCE with ferrites produces a drastic decrease in the R_{ct}, although this decrease is considerably more important when GCE is modified by the nanohybrid materials (MWCNT-MFe_2O_4 or TRGO-MFe_2O_4), demonstrating once more the synergism between ferrite NP and carbon nanostructures.

To obtain additional information about the catalytic activity of the nanomaterials towards hydrogen peroxide and evaluate the potential analytical application of GCE/nanohybrids, we also performed amperometric experiments at −0.400 V in a NaOH pH 13.00 solution for successive additions of hydrogen peroxide. The corresponding sensitivities are shown in Table 1. Compared to GCE/Naf-IP, the sensitivities for hydrogen peroxide reduction increases 2.9 and 3.7 times when GCE is modified with $CoFe_2O_4$ and $MnFe_2O_4$, respectively, as expected considering the catalytic activity of MFe_2O_4. The modification of GCE with MWCNT-$CoFe_2O_4$ and

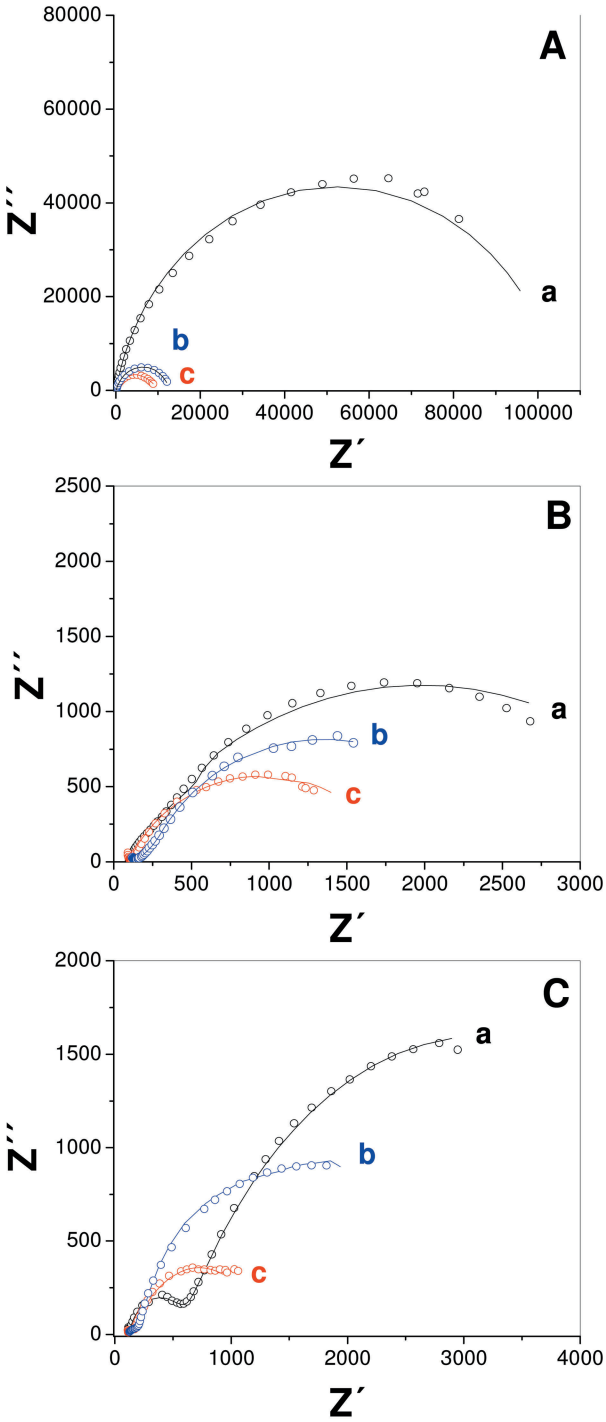

Fig. 3. Nyquist plots for the impedance spectra obtained for different electrodes: (A) GCE/Naf-IP (a) and GCE/MFe_2O_4 (Mn, b; Co, c) (B) GCE/MWCNT (a) and GCE/MWCNT-MFe_2O_4 , (Mn, b; Co, c) (C) GCE/TRGO (a) and GCE/TRGO-MFe_2O_4, (Mn, b; Co, c). Working potential: −0.400 V. Frequency range: 10 KHz to 10 mHz; Potential perturbation: 10 mV.

MWCNT-$MnFe_2O_4$ produced important enhancements of the sensitivities, which are even higher than the hypothetical sensitivities obtained by addition of the sensitivities for GCE/MWCNTs and GCE/MFe_2O_4. In fact, the values for GCE/MWCNTs-$CoFe_2O_4$ and GCE/MWCNTs-$MnFe_2O_4$ are 2.3 and 2.2 times higher than the values resulting from the addition of the sensitivities obtained with GCE/MWCNTs and GCE modified with the corresponding ferrite. A similar behavior is observed for GCE/TRGO-MFe_2O_4, with sensitivities 1.8 and 2.0 higher than the addition of the individual sensitivities for GCE/TRGO-$CoFe_2O_4$ and GCE/TRGO-$MnFe_2O_4$, respectively. Thus, in agreement with previous results, the synergism between $MnFe_2O_4$ and carbon nanostructures is also evidenced from the amperometric detection of hydrogen peroxide. Considering that the highest sensitivities were obtained for GCE/MWCNTs-$CoFe_2O_4$ and GCE/MWCNTs-$MnFe_2O_4$, we evaluated their short-term stability from amperometric experiments at −0.400 V using the same electrode surface. In the case of GCE/MWCNTs-$CoFe_2O_4$, the sensitivity (obtained from amperometric experiments for successive additions of hydrogen peroxide) remained in 95 % and 83 % of the original one for the second and third calibration plots, respectively. The sensitivity for the fourth calibration was 60 % and remained almost constant up to the tenth one. The average for ten sensitivities, given as percentage of the original one, was 71 %. In the case of GCE/MWCNTs-$MnFe_2O_4$, the sensitivities remained very close to the value obtained with the fresh electrode even after the calibration number 10, with an average of 91.3 % for the 10 successive calibrations.

Table 1. Sensitivities for hydrogen peroxide reduction obtained from amperometric recordings at −0.400 V in a 0.100 M NaOH solution pH 13.00 using different electrodes.

Electrode	Sensitivity ($\mu A\,mM^{-1}$)
GCE/Naf-IP	0.29 ± 0.03
GCE/MWCNT	1.03 ± 0.09
GCE/TRGO	1.18 ± 0.09
GCE/$CoFe_2O_4$	0.7 ± 0.1
GCE/$MnFe_2O_4$	0.9 ± 0.2
GCE/MWCNT-$CoFe_2O_4$	4.0 ± 0.4
GCE/MWCNT-$MnFe_2O_4$	4.2 ± 0.6
GCE/TRGO-$CoFe_2O_4$	3.3 ± 0.2
GCE/TRGO-$MnFe_2O_4$	2.1 ± 0.3

In summary, the significant changes in the maximum currents, R_{ct} and sensitivities for the reduction of hydrogen peroxide obtained at GCE/MFe_2O_4-carbon nanomaterials clearly indicate that the nanohybrids resulting from the association of MFe_2O_4 with MWCNT or TRGO facilitates the regeneration of M^{2+} at the carbon nanomaterials, producing a synergism in the catalytic reduction of hydrogen peroxide. This synergism makes MWCNTs-MFe_2O_4 and TRGO-MFe_2O_4 nanohybrids important analytical tools for the development of electrochemical (bio) sensors, not only for hydrogen peroxide quantification but also for the detection of other analytes based on the measurement of hydrogen peroxide reduction.

Experimental

Hydrogen peroxide and isopropanol (IP) were purchased from Merck. Nafion (Naf) was acquired from Sigma. Iron (99.5%), cobalt (99.9%) and manganese (99.5%) foils were obtained from Goodfellow. Multi-walled carbon nanotubes (MWCNTs, 5 μm length and (15 ± 5) nm diameter) were obtained from NanoLab and used as received. Graphene oxide (GO) was obtained from Graphenea. All the other chemicals were reagent grade and used without further purification.

Ultrapure water (ρ = 18 MΩ cm) from a Millipore-MilliQ system was used for preparing all the solutions. A NaOH solution pH 13.00 was employed as supporting electrolyte.

The electrosynthesis of ferrite nanoparticles (NPs) was performed with a potentiostat/galvanostat VersaStatTM EG&G Instruments from Princeton Applied Research. Amperometric experiments and LSV were performed with a PALM SENS potentiostat (4 channels EmStat 3). EIS experiments were performed with a CHI-650 potentiostat (CH Instruments).

A platinum wire and Ag/AgCl, 3 M KCl (CH Instruments) were used as counter and reference electrodes, respectively. All potentials are referred to the latter. A magnetic stirrer provided the convective transport during the amperometric measurements.

Synthesis of MFe_2O_4: Cobalt ($CoFe_2O_4$) and manganese ($MnFe_2O_4$) ferrite nanoparticles were prepared according to [39]. Briefly, two anodes, one of iron (2 cm^2) and the other of cobalt or manganese (2 cm^2) parallel positioned between them, and a cylindrical iron counter electrode (120 cm^2) were placed in a 0.040 M tetrabuthyl ammonium bromide aqueous solutions. Currents of 80 and 50 mA were applied for 1800 s to iron/cobalt or iron/manganese, respectively, to obtain cobalt or manganese ferrite NPs, both at room temperature. The resulting NPs were then stabilized and functionalized with citric acid according to [40].

The structural characterization of ferrite nanoparticles was carried out by X-ray powder diffraction using a Siemens D 5000 diffractometer, with a θ–2θ geometry, equipped with a primary and secondary monochromators and a SOL–X Bruker detector with a CuKα radiation. The morphological observations of the nanoparticles were performed by transmission electron microscopy (TEM) using a JEOL JEM 1010 operating at an accelerating voltage of 100 kV. The samples were prepared by dropping 10 μL of the ferrites dispersions onto copper grids coated with a carbon film and drying at room temperature. The amount of cobalt and manganese were obtained with an inductively coupled plasma optical emission spectrometer (ICP-OES) Perkin Elmer Optima 2100 DV.

Thermally reduced graphene oxide (TRGO) : GO was reduced by heating 100 mg at 950 °C for 30 s under nitrogen atmosphere. The resulting material was characterized by Raman spectroscopy, XPS and electrochemical techniques [41].

Preparation of the dispersions (MFe_2O_4-MWCNTs and MFe_2O_4-TRGO): 0.40 mg of carbon nanomaterials, either MWCNT or TRGO, were mixed with an amount of MFe_2O_4 equivalent to 0.1 mg of M and 500 μL of water/isopropanol (4:1), and then sonicated in an ultrasonic bath for 30 min. After sonication, 20 μL of commercial Nafion solution were added and sonicated for additional 30 min. Dispersions of carbon nanomaterials or ferrites were prepared in the same way by using 0.40 mg of MWCNT or TRGO or an amount of ferrites equivalent to 0.1 mg of M.

Preparation of GCE modified with the carbon nanomaterials-ferrite dispersion: GCEs were polished with alumina slurries of 1.0, 0.30, and 0.05 μm for 2 min each. Before functionalization, the electrodes were cycled in a 0.050 M phosphate buffer solution pH 7.40 for ten times from −0.300 V to 0.800 V at 0.050 $V s^{-1}$ and then modified by dropping 20 μL MWCNT-MFe_2O_4 (GCE/MWCNT-$CoFe_2O_4$ and GCE/MWCNT-$MnFe_2O_4$) or TRGO-MFe_2O_4 (GCE/TRGO-$CoFe_2O_4$ and GCE/TRGO-$MnFe_2O_4$). Once the solvent was evaporated at 50 °C, the modified electrodes were cycled ten times between −0.300 V and 0.800 V at 0.050 $V s^{-1}$ before starting the electrochemical experiments. GCEs were also modified with MFe_2O_4 (GCE/$CoFe_2O_4$ and GCE/$MnFe_2O_4$), MWCNT (GCE/MWCNT) or TRGO (GCE/TRGO) dispersions in a similar way. Control experiments were performed with GCE modified with 20 μL of water/isopropanol/Nafion solution (GCE/Naf-IP).

Polarization curves were obtained at 0.005 $V s^{-1}$ in deoxygenated 1.0×10^{-2} M hydrogen peroxide solutions. Amperometric measurements were conducted in a deoxygenated NaOH solution pH 13.00 by applying the desired working potential and allowing the transient currents to decay to a steady-state value prior to the addition of the analyte and subsequent current monitoring. EIS experiments were performed in the frequency range between 10 KHz and 10 mHz, with a potential perturbation of 10 mV and a working potential of −0.400 V using a 2.5×10^{-2} M hydrogen peroxide solution. The impedance spectra were analyzed by using the Z-view program. All measurements were performed in a deoxygenated 0.100 M NaOH pH 13.00 solution at room temperature.

Acknowledgements

The authors thank Proyecto Banco Santander-UAM. CONICET, SECyT-UNC, ANPCyT (Argentina). Fondecyt-Chile (1161117 and 1161225) and Project MINCYT (Argentina)-CONICYT (Chile) (CH/13/03 PCCI130050) and MAT2012-37109-C02-02 for the financial support.

References

[1] B. Halliwell, M. V. Clement, L. H. Long, *FEBS Lett.* **2000**, *4*, 10–13.

[2] L. H. Long, P. J. Evans, B. Halliwell, *Biochem. Biophys. Res. Commun.* **1999**, *262*, 605–609.
[3] R. Sharma, S. Bansal, S. Singhal, *RCS Advances* **2015**, *5*, 6006–6018.
[4] L. Yang, C. Xu, W. Ye, W. Liu, *Sens. Actuators B* **2015**, *215*, 489–496.
[5] A. A. Karyakin, E. A. Puganova, I. A. Budashov, I. N. Kurochkin, E. E. Karyakina, V. A. Levchenko, V. N. Matveyenko, S. D. Vartfolomeyev, *Anal. Chem.* **2004**, 76, 474–478.
[6] J. Liu, F. Lu, J. Wang, *Electrochem. Commun.* **1999**, *1*, 341–344.
[7] M. Somasundrum, K. Kirtikara, M. Tanticharoen, *Anal. Chim. Acta* **1996**, *319*, 59–70.
[8] J. Wang, G. Rivas, M. Chicharro, *Electroanalysis* **1996**, *8*, 434–437.
[9] H. Sakslund, J. Wang, O. Hammerich, *J. Electroanal. Chem.* **1996**, *402*, 149–160.
[10] M. S. Celej, G. A. Rivas, *Electroanalysis* **1998**, *10*, 771–775.
[11] G. Rivas, M. C. Rodríguez, *Electroanalysis* **2001**, *13*, 1179–1184.
[12] M. C. Rodríguez, G. A. Rivas, *Anal. Lett.* **2001**, *34*, 1829–1840.
[13] S. Miscoria, G. Barrera, G. Rivas, *Electroanalysis* **2002**, *14*, 981–987.
[14] S. A. Miscoria, G. D. Barrera, G. A. Rivas, *Electroanalysis* **2005**, *17*, 1578–1582.
[15] S. A. Miscoria, G. D. Barrera, G. A. Rivas, *Sens. Actuators B* 115, 205–211.
[16] K. Fang, Y. Yang, L. Fu, H. Zheng, J. Yuan, *Sens. Actuators B* **2014**, *191*, 401–407.
[17] G. L. Luque, M. C. Rodríguez, G. A. Rivas, *Talanta* **2005**, *66*, 467–471.
[18] Y. Pan, Z. Hou, W. Yi, W. Zhu, F. Zeng, Y-N. Liu, *Talanta* **2015**, *141*, 86–91.
[19] N. W. Beyene, P. Kotzian, K. Schachl, H. Alemu, E. Turkusic, A. Copra, H. Moderegger, I. Svancara, K. Vytras, K. Kalcher, *Talanta* **2004**, *64*, 1151–1159.
[20] E. Turkusic, J. Kalcher, E. Kahrovic, N. W. Beyene, H. Moderegger, E. Sofic, S. Begie, K. Kalcher, *Talanta* **2005**, *65*, 559–564.
[21] Z. Li, K. Gao, G. Han, R. Wang, H. Li, X. S. Zhao, P. Guo, *New J. Chem.* **2015**, *39*, 361–368.
[22] G. L. Luque, N. F. Ferreyra, G. Leyva, G. A. Rivas, *Sens. Actuators B* **2009**, *142*, 331–336.
[23] L. F. Liotta, F. Puleo, V. La Parola, S. G. Leonardi, N. Donato, D. Aloisio, G. Neri, *Electroanalysis* **2015**, *27*, 684–692
[24] F. N. Comba, M. D. Rubianes, L. Cabrera, S. Gutiérrez, P. Herrasti, G. A. Rivas, *Electroanalysis* **2010**, *22*, 1566–1572.
[25] F. N. Comba, F. Gutierrez, P. Herrasti, M. D. Rubianes, G. A. Rivas, *Electroanalysis* **2012**, *24*, 1541–1546.
[26] J. Jaime-González, E. Mazario, N. Menéndez, J. Sánchez-Marcos, A. Muñoz-Bonilla, P. Herrasti, *J. Solid State Electrochem.* **2016**, *20*, 1191–1198.
[27] S. Hazra, N. Ghosh, *J. Nanosci. Nanotechnol.* **2014**, *14*, 1983–2000.
[28] L. Cabrera, S. Gutierrez, N. Menendez, M. P. Morales, P. Herrasti , *Electrochim. Acta* **2008**, *53*, 3436–3441.
[29] E. Mazarío, P. Herrasti, M. P. Morales, N. Menendez, *Nanotechnology* **2012**, *23*, 355708.
[30] N. Yang, G. M. Swain, X. Jiang, *Electroanalysis* **2016**, 28, 27–34.
[31] G. A. Rivas, M. C. Rodríguez, M. D. Rubianes, F. A. Gutierrez, M. Eguílaz, P. R. Dalmasso, E. Primo, C. Tettamanti, M. L. Ramírez, A. Montemerlo, P. Gallay, C. Parrado, *App. Mat. Today* **2017**, *9*, 566–588.
[32] J. Molina, F. Cases, L. M. Moretto, *Anal. Chim. Acta* **2016**, *946*, 9–39.
[33] A. Walcarius, S. D. Minteer, J. Wang, Y. Lin, A. Merkoci, *J. Mater. Chem. B* **2013**, *1*, 4878–4908.
[34] B. Borisova, M. L. Villalonga, M. Arévalo-Villena, A. Boujakhrout, A. Sánchez, C. Parrado, J. M. Pingarrón, A. Briones-Pérez, R. Villalonga, *Anal. Bioanal. Chem.* **2017**, *409*, 5667–5674.
[35] S. K. Kandasamy, K. Kandasamy, *J. Inorg. Organomet. Polym. Mater.* **2018**, *in press.* doi.org/10.1007/s10904-018-0779-x
[36] T. Ravindran Madhura, P. Viswanathan, G. Gnana Kumar, R. Ramaraj, *J. Electroanal. Chem.* **2017**, *792*, 15–22.
[37] A. Ensafi, H. A. Alinajati, M. Jafari-Asl, B. Rezaei, F. Ghazaei, *Mat. Sci. and Eng. C* **2016**, *60*, 276–284.
[38] H. Teymourian, A. Salimi, S. Khezrian, *Biosens. Bioelectron.* **2013**, *49*, 1–8.
[39] E. Mazarío, J. Sánchez-Marcos, N. Menéndez, M. Cañete, A. Mayoral, S. Rivera-Fernández, J. M. de la Fuente, P. Herrasti, *Phys. Chem. C* **2015**, *119*, 6828–6834.
[40] E. Mazario, N. Menéndez, P. Herrasti, M. Cañete, V. Connord, J. Carrey, *J. Phys. Chem. C* **2013**, *117*, 11405–11411.
[41] D. F. Báez, H. Pardo, I. Laborda, J. F. Marco, C. Yáñez, S. Bollo, *Nanomaterials* **2017**, 168

Received: March 15, 2018
Accepted: April 6, 2018
Published online on April 25, 2018

